Supplementary Information

Field-like spin-orbit torque induced by bulk Rashba channel in GeTe/NiFe bilayers

Jeehoon Jeon, Seong Won Cho, OukJae Lee, Jinki Hong, Joon Young Kwak, Seungwu Han, Soonho Jung, Yunseok Kim, Hye-Won Ko, Suyoun Lee, Kyung-Jin Lee & Hyun Cheol Koo

Contents

Supplementary Note 1. Magneto-transport properties of epitaxial GeTe thin films

Figure 1(f) shows the MR vs. *H* curves of the 50 nm-thick GeTe film with a Se capping layer (20 nm) at various temperatures. It shows a downward cusp near zero magnetic field, suggesting the quantum correction to MR due to the weak antilocalization (WAL[1-4]). To evaluate the spin-orbit coupling strength, we have analyzed the MR(*B*) curve using three-dimensional (3D) Fukuyama-Hoshino (F-H) model[3-5] as follows.

$$\frac{\Delta\rho_{WAL}(B)}{\rho(0)^2} = \frac{e^2}{2\pi^2 h}\sqrt{\frac{2\pi eB}{h}}\left[\frac{1}{2}f_3\left(\frac{B}{B_\phi}\right) - \frac{3}{2}f_3\left(\frac{B}{B_2}\right)\right], \quad (1)$$

$$f_3(y) = \sum_{n=0}^{\infty}\left[2\left(n+1\frac{1}{y}\right)^{\frac{1}{2}} - 2\left(n+\frac{1}{y}\right)^{\frac{1}{2}} - \left(n+\frac{1}{2}+\frac{1}{y}\right)^{-\frac{1}{2}}\right]. \quad (2)$$

Here, *e* and *h* are the elementary charge and the Planck constant, respectively. The fitting parameters B_ϕ and B_2 are given by $B_\phi = B_i + 2B_s$ and $B_2 = B_i + \frac{2}{3}B_s + \frac{4}{3}B_{so}$, where B_i, B_s and B_{so} characterize the strength of inelastic, magnetic spin-flip, and spin-orbit scatterings, respectively. Assuming no magnetic impurity inducing spin-flip scatterings ($B_{so} = 0$), the B_ϕ and B_{so} can be obtained by fitting equation (1) to the experimental MR curves [black dashed lines in Fig. 1(f)]. From the fitting parameter, Rashba constant ($\alpha_R = \frac{\sqrt{e\hbar^3 B_{so}}}{m}$) is estimated to be ~ 0.3×10^{-10} eV·m at 20 K, which is about three times larger than that of strong semiconductor Rashba system[6].

It is however smaller than ~4.2×10^{-10} eV·m obtained from the SARPES measurement of the 200 nm-thick GeTe thin film grown on BaF_2[7]. It is mainly attributed to the difference in the ways of measuring α_R in SARPES and WAL. While α_R obtained by the SARPES measurement is the maximum in the well-defined direction in the momentum space, α_R in this work is obtained from the transport measurement giving the momentum-average value. Another possibility is the difference in the composition of GeTe thin film used in the SARPES and this work. In a previous report[8], it was reported that the spin-split surface band disappeared in a relatively Ge-rich GeTe ($Ge_{0.46}Te_{0.54}$) sample whereas it was clearly observed in a Te-rich sample ($Ge_{0.39}Te_{0.61}$), implying that the spin-split surface band is sensitive to the composition of GeTe. Considering that the composition of our GeTe thin film is close to Ge:Te = 1:1, it might be an origin of the small α_R observed in this work.

Supplementary Note 2. Estimation of SOTs using spin torque ferromagnetic resonance (ST-FMR)

We estimated the DLT- and FLT-efficiencies for GeTe/NiFe bilayers using ST-FMR method. For this, we utilized a structure consisting of substrate/GeTe(20 nm)/NiFe(11 nm)/MgO(2 nm)/Ta(2 nm). Fabrication of the device and ST-FMR measurement were performed in the same ways as described in the reference[9]. In the estimation, we used the following equation to determine the θ_{DL} and θ_{FL+Oe}. The symmetric (antisymmetric) voltage part of the ST-FMR signal ($V_{S(A)}^{mix}$) originates from DLT (FLT+OeT) which is given by

$$V_{S(A)}^{mix} = -I_{rf}^2 \frac{\gamma}{4} \Delta R_{AMR,eff} \left[\frac{\sin 2\varphi \cos\varphi}{\Delta \cdot 2\pi \cdot (df/dH)_{H_o}} \right] \left[\frac{\hbar}{2e} \frac{1}{M_s t_{NiFe}} \right] \left[\frac{1}{w \cdot t_{GeTe}} \right] \theta_{DL(FL+Oe)} \quad (3)$$

where $\varphi = \pi/4$ in our measurements and Δ is a half width at half maximum. The RF current through the device (I_{rf}) was estimated for a given RF power and frequency using a vector network analyzer (VNA) and taking into account the loss factors. Effective AMR ($\Delta R_{AMR,eff}$) were also measured separately. Figure S8 (a) shows the measured spectra and (b) the estimated θ_{DL} and θ_{FL+Oe} from the GeTe/NiFe layer as a function of the frequency. The averaged θ_{DL} is +0.06±0.007 while θ_{FL+Oe} = +0.11±0.02. Since the $\theta_{Oe} = (e/\hbar) M_S t_{NiFe} t_{GeTe}$ = +0.34, we have $\theta_{FL} = -0.23 \pm 0.02$. The averaged spin Hall efficiencies (θ_{DL} = +0.06 and θ_{FL} = -0.23) correspond to ρ_{DL} = –0.23 mT/(10^7 Acm^{-2})

and B_{FL}/J = –0.9 mT/(10^7 Acm^{-2}), respectively. These values are not exactly the same as those in Fig. 3(c), but are consistent with the in-plane second harmonic measurements within the magnitude of factor two. This result is in agreement with the in-plane second harmonic measurement, i.e. the negative sign and large magnitude of the FLT in GeTe/NiFe bilayers.

Supplementary Figures

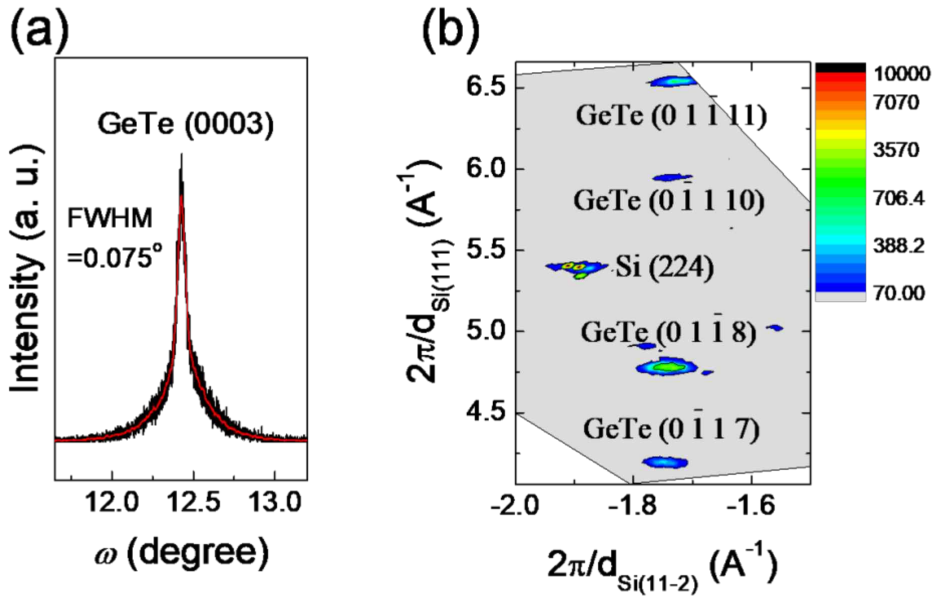

Fig. S1 X-ray diffraction (XRD) of α-GeTe thin film on Si(111) substrate. a Rocking curve of α-GeTe (0003) peak. **b** Reciprocal lattice mapping around Si(224) peak.

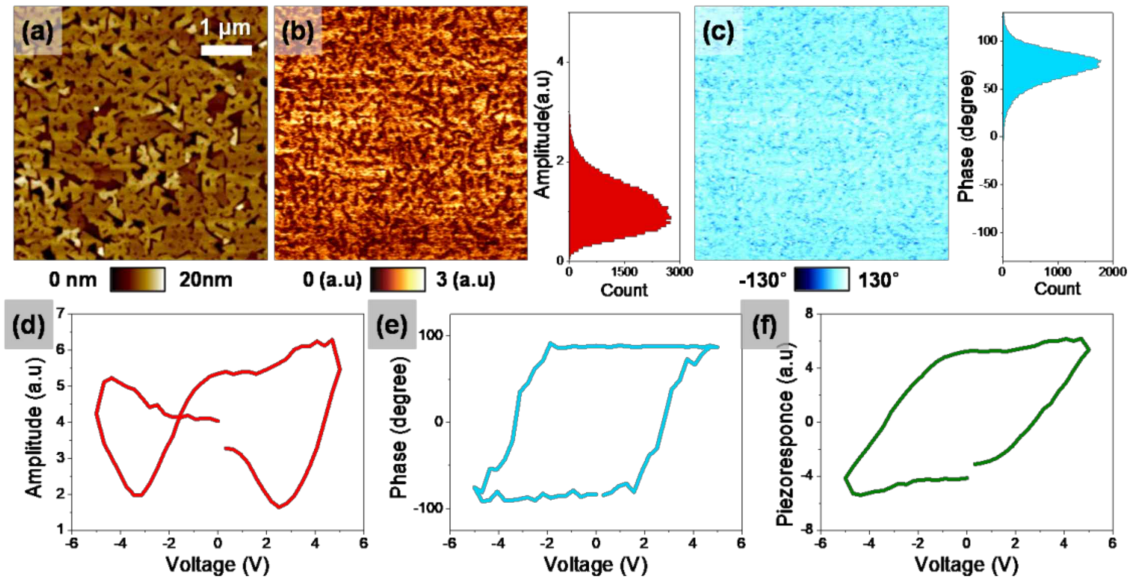

Fig. S2 Surface profile and ferroelectric property a Topography image, **b** (Piezoresponse force microscopy) PFM amplitude and corresponding histogram, and **c** PFM phase image and corresponding histogram of α-GeTe thin film. PFM **d** amplitude, **e** phase, and **f** piezoresponse hysteresis loops of α-GeTe thin film. Those hysteresis loops can show polarization switching depending on DC voltage applied to the atomic force microscopy (AFM) tip.

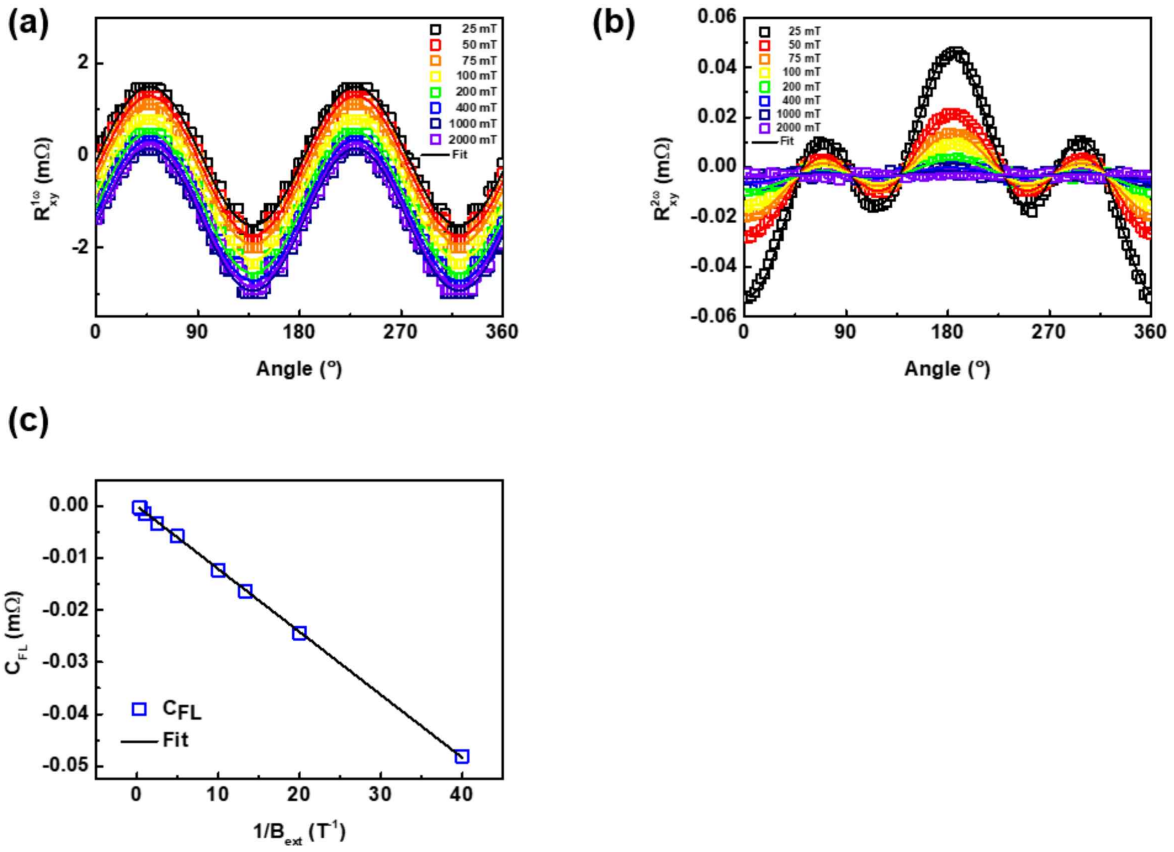

Fig. S3 Experimental determination of the sign of current-induced Oersted field using Cu(20 nm)/NiFe(10 nm) bilayer. a, b Transverse resistances for first (**a**) and second Harmonic measurements (**b**) with I_{AC} = 10 mA. **c** Amplitude of C_{FL} term in Cu/NiFe bilayer, as a function of B_{ext}^{-1}, which shows that the B_{Oe} has negative sign which is same as that in GeTe/NiFe bilayer.

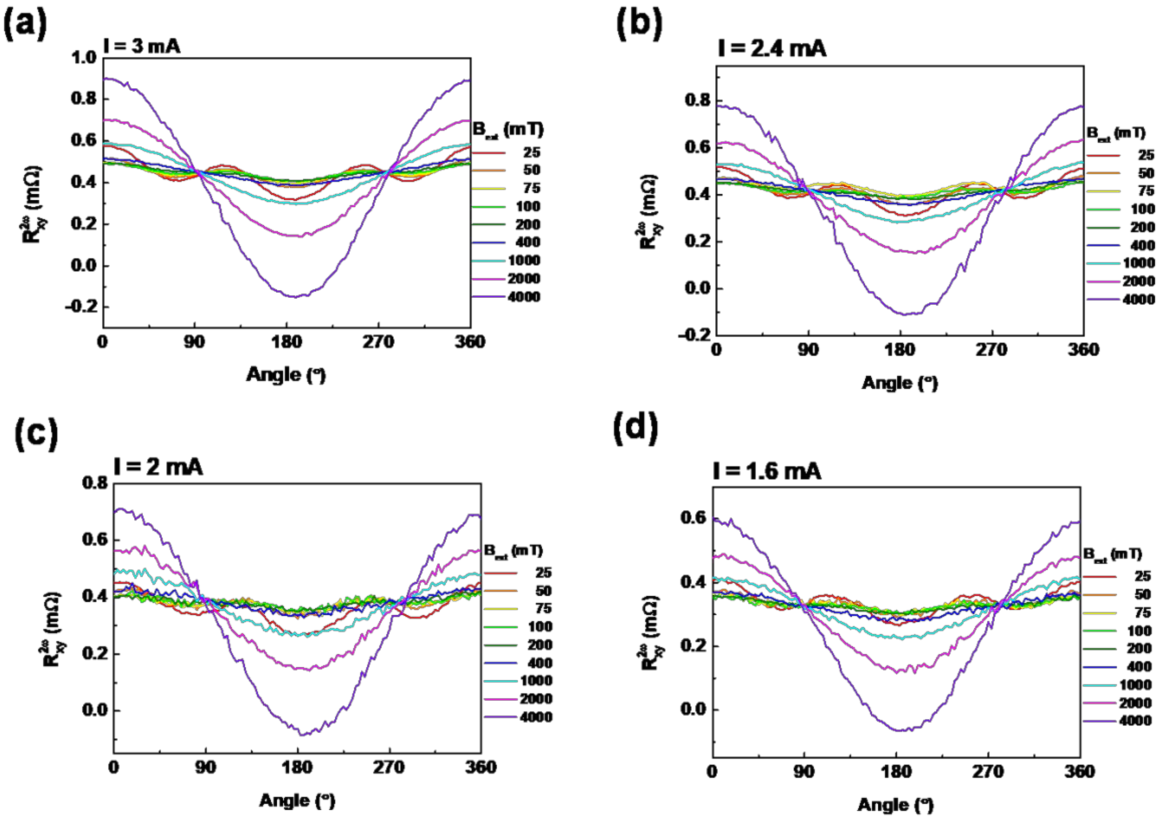

Fig. S4 Second harmonic resistances as a function of bias current. a *I* = 3 mA. **b** *I* = 2.4 mA. **c** *I* = 2 mA. **d** *I* = 1.6 mA.

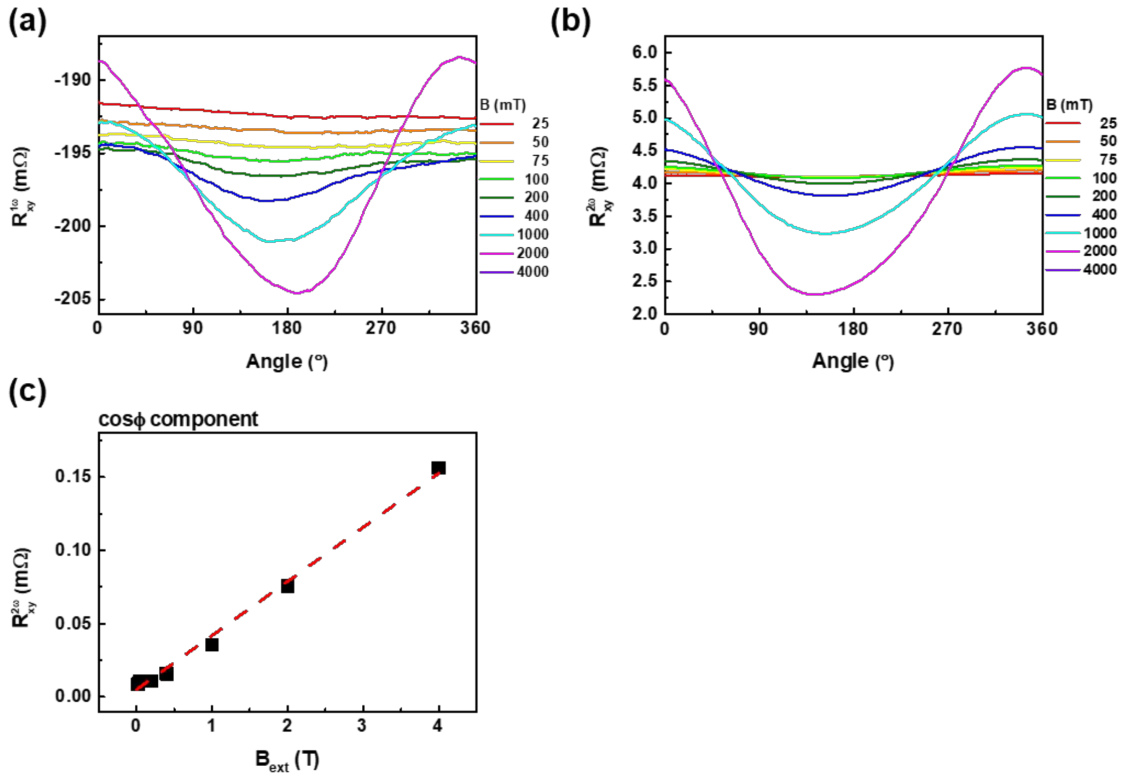

Fig. S5 Harmonic resistances in a GeTe/Cu structure. a, **b** Transverse resistances for first (**a**) and second harmonic measurements (**b**). **c** $\cos\varphi$ component in second harmonic measurement. In second harmonic resistance, $\cos2\varphi\cos\varphi$ term does not exist which means there is no field-like torque but only thermal related contribution. In general, there is no damping-like torque in the system which does not possess field-like torque. The conductivity of Cu is much higher than GeTe, but GeTe is much thicker than Cu. Consequently, the substantial current flows into the GeTe for evaluating 2nd harmonic signal. Actually, the current density of GeTe layer in a GeTe/Cu structure is 2.47 × 10^9 A/m^2 which is almost same as the current density of GeTe layer in a GeTe/NiFe structure (2.79 × 10^9

A/m^2). Thus, the control experiment using GeTe/Cu device is valid to compare with GeTe/NiFe device.

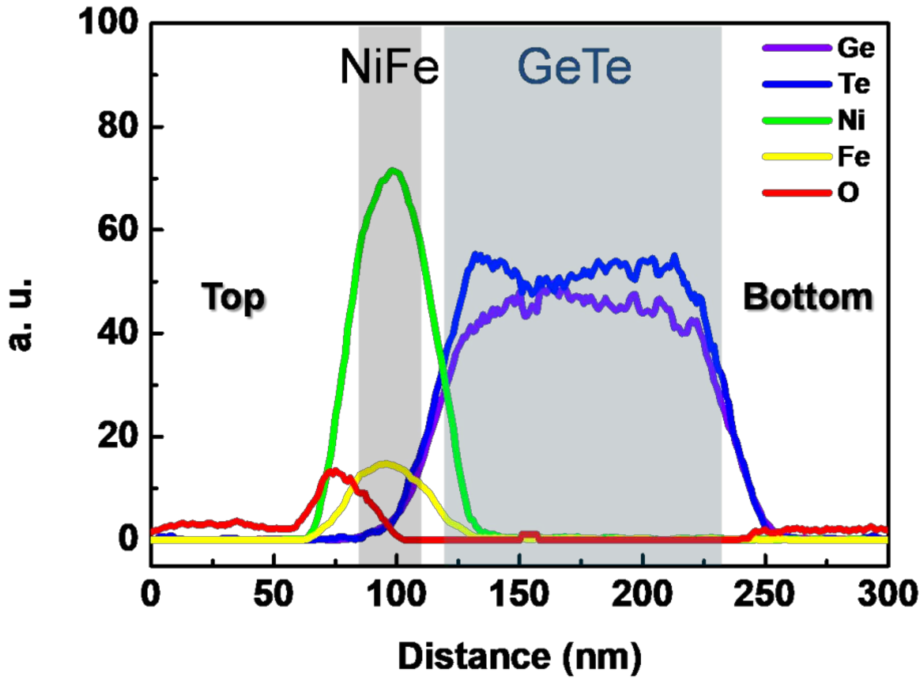

Fig. S6 Energy dispersive X-ray spectroscopy (EDS) analysis of multilayer. Energy dispersive X-ray spectroscopy (EDS) analysis of multilayer. The structure (from top) consists of SiNx (200 nm). TiOx (2 nm), NiFe (20 nm), GeTe (120 nm) and Si substrate. Oxygen was hardly detected at the interface between NiFe and GeTe layers.

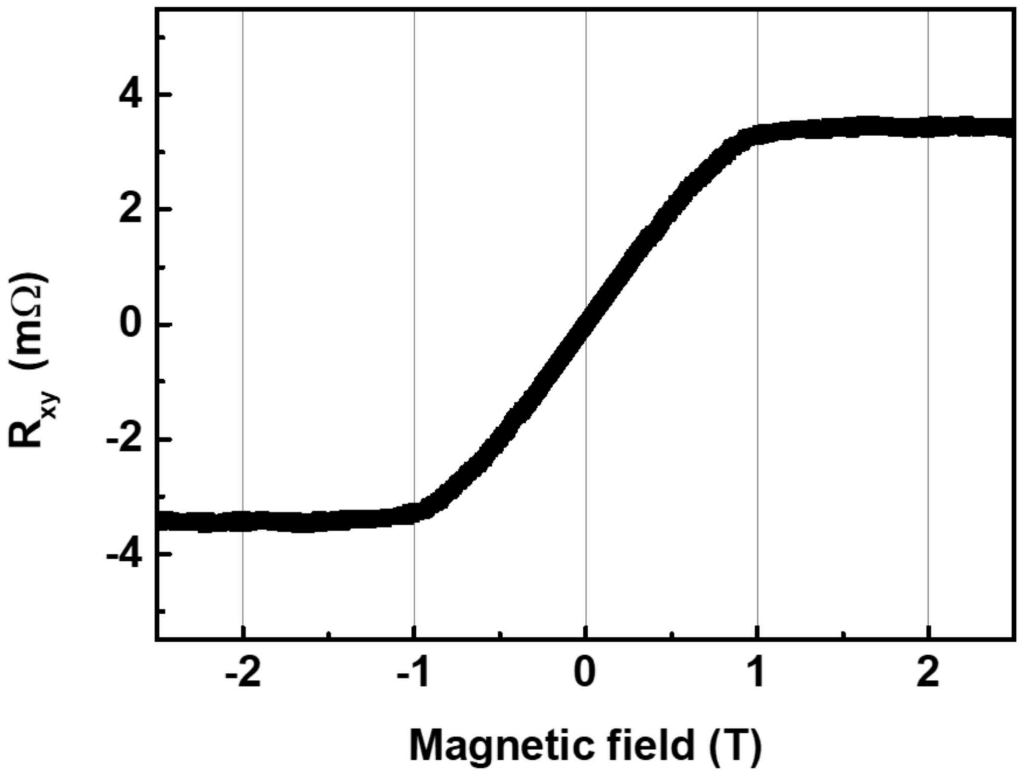

Fig. S7 Anomalous Hall measurement of $Ni_{81}Fe_{19}$. The signal magnitude is anomalous Hall resistance and saturation field is the effective demagnetizing field, $B_{dem}-B_{ani}$, where B_{dem} is the demagnetizing field and B_{ani} is the sample-dependent perpendicular anisotropy field.

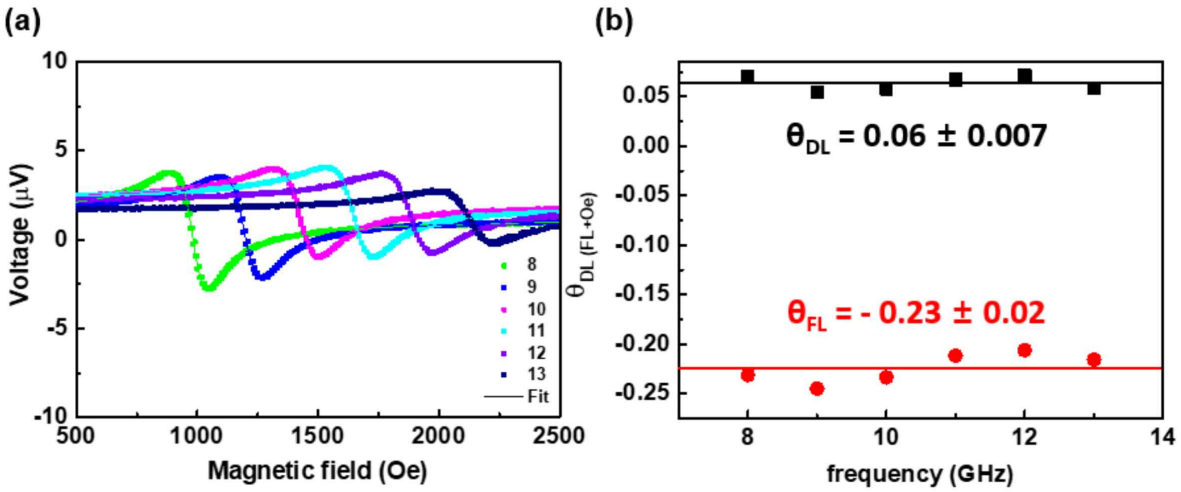

Fig. S8 Spin-torque ferromagnetic resonance (ST-FMR). a Measured ST-FMR signals from a GeTe(20 nm)/NiFe(11 nm) device at room temperature. **b** Estimated SOT efficiencies (θ_{DL}, θ_{FL}) as a function of frequency.

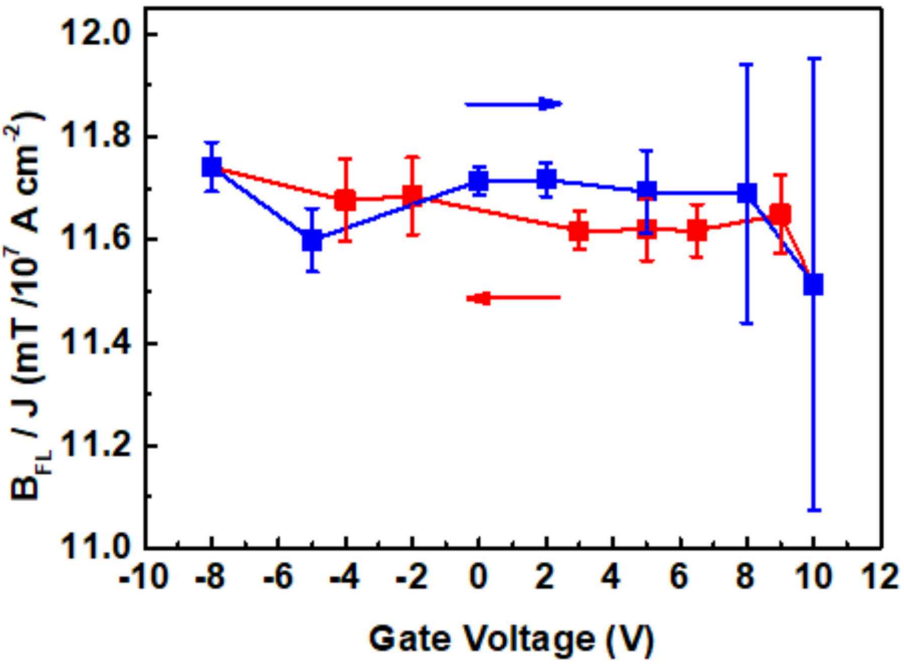

Fig. S9. Gate modulation of field-like torque.

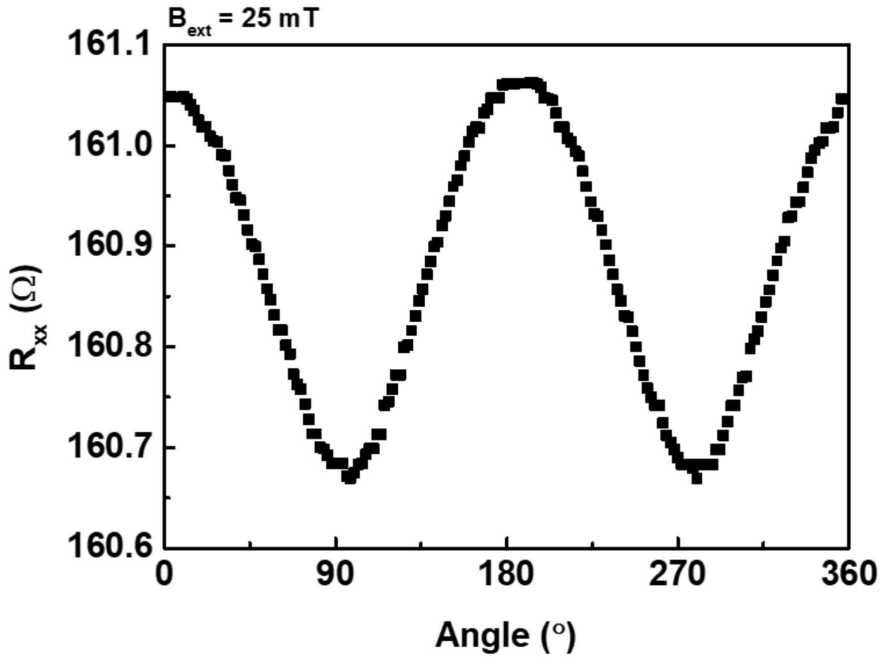

Fig. S10 Longitudinal resistance as a function of the azimuthal angle of the in-plane magnetic field.

Supplementary References

1. Altshuler, B. L., Khmel'nitzkii, D., Larkin, A. I. & Lee, P. A. Magnetoresistance and Hall effect in a disordered two-dimensional electron gas. *Phys. Rev. B* **22**, 5142–5153 (1980).
2. Datta, S. *Electronic Transport in Mesoscopic Systems*. (Cambridge University Press, 1997).
3. Hikami, S., Larkin, A. I. & Nagaoka, Y. Spin-Orbit Interaction and Magnetoresistance in the Two Dimensional Random System. *Prog. Theor. Phys.* **63**, 707–710 (1980).
4. Hu, J., Liu, J. Y. & Mao, Z. Q. Spin–orbit coupling and weak antilocalization in the thermoelectric material β-$K_2Bi_8Se_{13}$. *J. Phys.: Condens. Matter* **26**, 095801 (2014).
5. Fukuyama, H. & Hoshino, K. Effect of Spin-Orbit Interaction on Magnetoresistance in the Weakly Localized Regime of Three-Dimensional Disordered Systems. *J. Phys. Soc. Jpn.* **50**, 2131–2132 (1981).
6. Koo, H. C. *et al.* Control of Spin Precession in a Spin-Injected Field Effect Transistor. *Science* **325**, 1515–1518 (2009).
7. Krempaský, J. *et al.* Disentangling bulk and surface Rashba effects in ferroelectric α -GeTe. *Phys. Rev. B* **94**, (2016).
8. Rinaldi, C. *et al.* Ferroelectric Control of the Spin Texture in GeTe. *Nano Lett.* **18**, 2751–2758 (2018).
9. Kim, J. *et al.* Spin-orbit torques associated with ferrimagnetic order in Pt/GdFeCo/MgO layers. *Sci. rep.* **8**, 1-8 (2018).